

# Cluster morphology in magneto-rheological fluids: fractal dimensions during anisotropic aggregation and disaggregation processes.

Pablo Domínguez-García,<sup>1</sup> Sonia Melle,<sup>2</sup> and Miguel A. Rubio<sup>1</sup>

<sup>1</sup>Dep. Física Fundamental, UNED, Senda del Rey 9, Madrid 28040, Spain.\*

<sup>2</sup>Dep. Óptica, Universidad Complutense de Madrid, Arcos de Jalón s/n 28037 Madrid, Spain.†

(Dated: May 26, 2019)

We study the evolution of the fractal dimensions during anisotropic aggregation and disaggregation (i.e., when the applied field is switched off) processes, in a magneto-rheological fluid composed by super-paramagnetic particles with a diameter of 1 micron, suspended in water under the action of a constant uniaxial magnetic field. We use video-microscopy and image analysis to retrieve the form of the aggregates and calculate the following fractal dimensions: one-dimensional  $D_1$ , two-dimensional  $D_2$ , perimeter-based fractal dimension  $D_p$  and two-dimensional capacity dimension or box-counting dimension  $D_B(2D)$ . We apply this methodology for different values of the magnetic field amplitude and particle concentration. During aggregation, we can calculate an average value  $\langle D_p \rangle \sim 1.84$  for the rod-like chains and we find a linear dependence of the capacity dimension with the ratio of two characteristic length scales. By means of a quantification of the roughness, we interpret  $D_p$  as a measure of the clusters border roughness, while the capacity dimension represents how the chains fill the space. We also show how the quadratic deviation of the cluster contour height follows power-law behaviours in the initial stages of aggregation and disaggregation. We compare our results on projected fractal dimensions with previous theoretical and experimental studies about aggregation of magnetic particles. As a result, we check some recently proposed theoretical relation between  $D_p$  and the three-dimensional fractal dimension  $D_f$ .

PACS numbers: 61.43.Hv, 83.80.Gv, 82.70.-y

## I. INTRODUCTION.

The study of fractal geometry [1, 2] aiming to characterize the morphology of aggregates has been a wide and diverse research field on mathematics, chemistry, physics and biosciences along the last decades. For example, the concepts of fractal geometry have been useful in fields as diverse as the study of cancer growth and cell structure [3, 4] and the distribution of galaxies [5]. In the last three decades, several experimental studies about colloidal aggregation have been carried out aiming to determine fractal dimensions of colloidal aggregates, in special, by means of light scattering techniques [6, 7, 8]. The interest to determine fractal dimension of aggregates is related to the practical applications. In fact, by means of fractal dimension analysis, dynamic or morphological properties of aggregates can be investigated in processes relevant for water depuration, biology, medicine or engineering. For instance, properties such as deposition, sedimentation [9, 10], settling [11, 12], roughness [13], coagulation or porosity (see references on [14]), have been analysed in terms of fractal concepts. Two main classes of optical techniques are widely used in the study of the morphology of the aggregates in colloid science: light scattering techniques [15] and direct imaging techniques (e.g., video-microscopy) [16]. Hereafter, we will study 2D-projected fractal dimensions by means

of image analysis in an experimental colloidal system, namely, a magneto-rheological fluid (MRF). We use an aqueous suspension of micron-sized super-paramagnetic particles that, under the action of a constant uniaxial magnetic field, acquire a magnetic dipole moment that forces them to aggregate into linear chains [17, 18, 19, 20]. Magnetic particles [21, 22, 23], magneto-rheological fluids [24, 25, 26], organic-solvent-based magnetic fluids [27] or magnetic liposomes [28] have been the object of several experimental investigations on fractal aggregation [29, 30] and fractal geometry. Studies on fractal dimension by means of simulations have been also developed on magnetic particles [21, 31] or two-dimensional magnetic fluids simulations including van der Waals and electrostatic forces [32]. In this paper, we use 2D images of the colloidal aggregates in a MRF to compute 2D-projected values of the fractal dimension of the aggregates. These projected fractal dimension gives a lot of information concerning the morphology and spatial properties of the clusters. Regarding fractal properties, many of the experimental works for magnetic particle aggregation commented before, give different information: light scattering techniques yield fractal dimension values related to the three-dimensional (3D) structure of the aggregate distribution, while direct imaging techniques usually deal with two-dimensional (2D) projected images of the real three-dimensional structure of the aggregate distribution. However, some progress in this direction has been recently done [33], and several possible relations have been theoretically found [34, 35, 36]. We perform a detailed analysis of these studies on Section VI.

\*Electronic address: pdominguez@fisfun.uned.es

†Electronic address: smelle@fis.ucm.es

The structure of the paper is as follows: after the In-

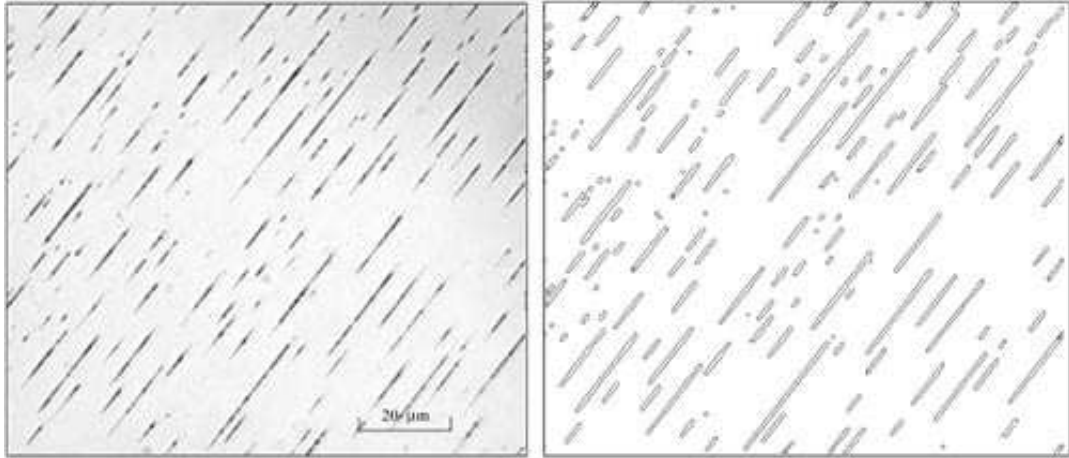


FIG. 1: Example of image analysis. Chains formed by super-paramagnetic micro-particles after  $t = 4158.4$  s of constant applied field with  $\lambda = 1688$  and  $\phi_{2D} = 0.088$ . Left: original captured image. Right: corresponding analysed binary image.

introduction, Section II contains a description of the experimental setup and procedure. In Section III we include a brief recall on the definitions of the several fractal dimensions that will be used throughout the paper, including practical details about the computational methods. Section IV contains the description of the results and Section V displays some conclusions and prospects for future work.

## II. MATERIALS AND METHODS

### A. Experimental Setup.

Our magneto-rheological sample consists on a commercial aqueous suspension of super-paramagnetic particles, (Estapor M1-070/60). These particles are composed by a polystyrene matrix with embedded magnetite crystals ( $Fe_3O_4$ ) of small diameter (10 nm). Since these iron oxide grains are randomly oriented inside the micro-particles, the resulting average magnetic moment is negligible in the absence of an external magnetic field. The super-paramagnetic particles have a radius  $a = 0.48 \mu m$  and a density  $\rho \sim 1.85 g/cm^3$  with a magnetic content of 54.7%.

The particles are denser than water and, therefore, they sediment to the bottom of the container. The height probability distribution of the particles can be calculated [37] and, for the particles here used, it can be shown that 80 % of the particles lie in a narrow layer above the bottom glass plate, with a thickness of, approximately, twice the particle diameter. Hence, most of the particles are captured with a narrow field depth optical system, and the images correspond to an effective two-dimensional system.

The surface of the latex micro-spheres is functionalized with carboxylic groups. The suspension has been

also provided with a 1 g/l concentration of a surfactant (sodium dodecyl sulfate). For these kind of suspensions we have measured a zeta potential by means of a Malvern Zetasizer Nano, obtaining values in between  $-110$  mV and  $-60$  mV for suspension pH in the range 6 – 7, reflecting the presence of an electrostatic repulsive force in the system.

The suspension sample is confined in a cylindrical cell, with a diameter of 6.5 mm and a height of 100  $\mu m$ , made of two quartz windows separated by a teflon spacer. A water jacket connected to a circulation thermostatic bath keeps the temperature constant during the experiments to  $T = 282 \pm 1$  K. The system used to generate the magnetic field is composed by a pair of coils fed by a power amplifier (BOP-50-4M) driven by a programmable arbitrary function generator (HP-33120A). This system allows for the generation of an uniform magnetic field along the measurement region (see more details about the experimental system on [38]). The video-microscopy setup used to record the images is located below the sample, and is formed by a long working distance microscope (Navitar) with zoom capabilities attached to a CCD camera (Retiga-Ex) with 12 bit intensity resolution and  $1360 \times 1036$  px spatial resolution. The required illumination is generated from the top using an optical fiber Fostec light source. Full frame images are captured every 0.4 seconds during a total time of approximately 8000 seconds at maximum spatial resolution.

### B. Experimental procedure.

The control parameters in the experiments are the volume fraction of the suspension and suitably defined dimensionless magnetic interaction energy. Actually, when an external magnetic field  $\vec{H}$  is applied, the particles acquire a magnetic dipole moment aligned with

the external field direction. This magnetic moment is  $\vec{m} = (4\pi/3)a^3\vec{M}$ , where  $\vec{M} = \chi\vec{H}$ , being  $\vec{M}$  the magnetization of the particle, and  $\chi$  the particle's magnetic susceptibility. The relevant parameter in the study of these suspensions is the ratio between the magnetic interaction energy for two particles in contact,  $W_m$  and the energy of thermal fluctuations,  $k_B T$ :

$$\lambda \equiv \frac{W_m}{k_B T} = \frac{\mu_0 m^2}{16\pi a^3 k_B T} \quad (1)$$

where  $\mu_0$  is the vacuum magnetic permeability,  $k_B$  the Boltzmann constant, and  $T$  the temperature. The values of  $\lambda$  in the experiment have been calculated from the magnetization curve of the particles that was obtained by means of a vibrating sample magnetometer. The value obtained for the saturation magnetization was 46.5 emu/g.

The volume fraction of particles  $\phi$  in the solution is defined as the fraction of the volume occupied for the particles over the total volume of the solution. For the purpose of this study, it is more useful to use an effective surface fraction which is calculated by dividing the sum of the area of all cluster contained in the image by the image total area. Hereafter,  $\phi_{2D}$  will refer to this effective surface fraction.

These parameters,  $\lambda$  and  $\phi_{2D}$ , can be used to define two characteristic length scales. First, we can define a distance,  $R_1$ , at which the dipole-dipole interaction energy is equal to the energy of thermal fluctuations, i.e.,  $R_1 \equiv 2a\lambda^{1/3}$ . Second, we may define an initial average inter-particle distance,  $R_0 \equiv 2a\phi_{2D}^{1/2}$ . The ratio of these two length scales allows us to distinguish between diffusion limited and field driven aggregation processes. If at the time the field is switched on  $R_1 < R_0$ , the aggregation process should be diffusion limited, while if  $R_1 > R_0$ , the aggregation process should be field driven.

The sedimentation velocity for the particles in the suspension can be calculated from the buoyancy force as  $v \approx (2a^2g(\rho - \rho_s))/(9\eta)$ , where  $g$  is the gravity constant, and  $\eta$  and  $\rho_s$  are the viscosity and density of the solvent, respectively. Thus the sedimentation velocity in our experiment is 0.43  $\mu\text{m}/\text{s}$ .

When the sample cell containing the magnetic suspension is introduced in the experimental setup, it is left at least 15 minutes to equilibrate without external field, to allow for particle sedimentation and temperature stabilization. After this time, most of the particles lay in a thin layer of 2 particles diameter depth, located right above the bottom quartz window.

After this equilibration time, we capture images during 5 minutes without field and then, a constant uniform magnetic field is switched on. The field triggers the aggregation process and, images are recorded during the time the field is being applied (approximately, 5000 seconds). Then, we switch off the magnetic field and capture another hour of images during the disaggregation process of the previously formed chains. Hence, we record approximately 21000 images for each experiment.

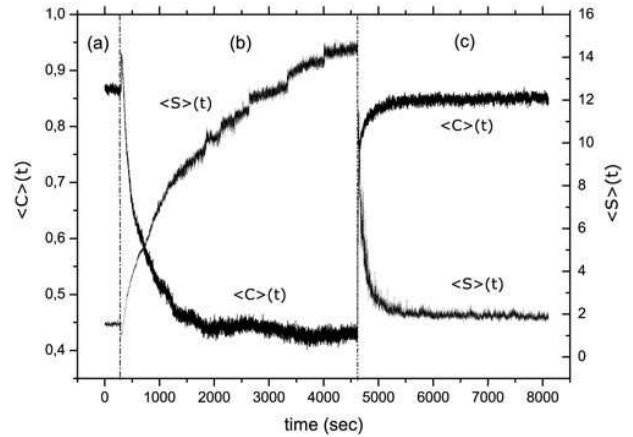


FIG. 2: Temporal evolution of mean cluster circularity  $\langle C \rangle(t)$  and mean cluster size  $\langle S \rangle(t)$  for a case of  $\lambda = 1688$  and  $\phi_{2D} = 0.088$ . The magnetic field is applied at  $t = 300$  s ((a) region without field and (b) region with field where occurs the aggregation process) and disconnected at  $t = 4620$  s ((c) region without field and disaggregation process).

This procedure is performed in experiments carried out at different values of  $\lambda$  and  $\phi_{2D}$ . The image analysis, data extraction and statistical calculations have been carried out with image processing software developed at our lab, based in the *ImageJ*[39] free open source Java program for image analysis. In this software, we have implemented an adaptative threshold image processing algorithm that removes the image background and suitably captures the contour of the clusters. An example of a filtered image can be seen in Fig.1. The contour of each cluster is then used to calculate geometrical properties such as cluster perimeter,  $P$ , area,  $A$ , Feret's diameter (longest distance between cluster contour points),  $l_f$ , and circularity,  $C = 4\pi A/P^2$ .

Moreover, we have calculated the cluster size probability density,  $n_s(t)$ , which is the number of clusters of size  $s$ , per unit area, present in the system at time  $t$  [40]. Then,  $n_s(t)$ , is used to calculate the average cluster size  $S(t) = \sum_s s^2 n_s(t) / \sum_s s n_s(t)$ .

### III. FRACTAL DIMENSION USING IMAGE ANALYSIS.

A fractal object presents self-similarity, i.e., when we change the scale where the object is observed, the result is very similar or identical to the original observed one. It is possible to classify fractals according to the variations of this property. From a rigorous point of view, a fractal can be defined as a set of points whose Hausdorff dimension is larger than its topological dimension. In general, if we have a fractal quantity  $F$ , it is connected with a length  $l$  using a relation such as  $F \sim l^{D_C}$ , where  $D_C$  is the fractal dimension associated with this fractal quantity. By means of fractal dimension,  $D_f$  (also called

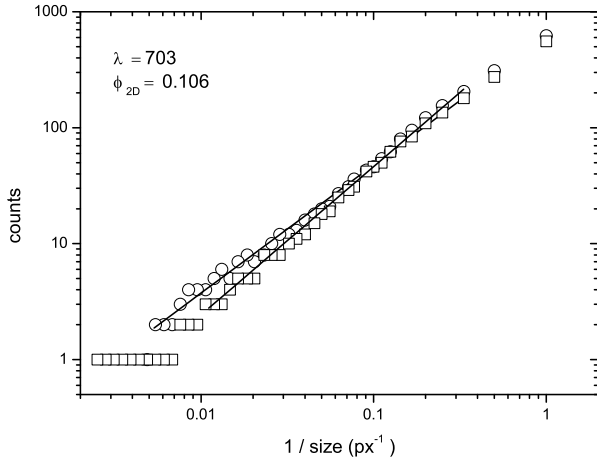


FIG. 3: Log-log plots of number of counts versus the inverse of the box size for a box-counting method. Box sizes on the log-log plots are powers of 2, so the points on the graphs are equally spaced. We use a chain during aggregation ( $t = 4989.6$  s) and during disaggregation (10 s after the field has been switched off) for an experiment with  $\lambda = 703$  and  $\phi_{2D} = 0.106$ . In the first case we obtain  $D_B(2D) = 1.11 \pm 0.02$  and  $D_B(2D) = 1.28 \pm 0.02$  in the second.

$D_3$  or  $D$ ), an interpretation can be made on how the aggregate fills the space or how primary particles fill the space of the volume occupied by the aggregate. An usual method to determine the fractal dimension of an aggregate knowing its number of particles,  $N$ , is through the radius of gyration,  $R_g$  [29]. Then, the following expression is verified:

$$R_g(N) \sim N^{1/D_f} \quad (2)$$

This is a very reliable method for determining  $D_f$ , if the number of particles for cluster is known with enough precision, being widely used in colloidal aggregation [41]. However, it is usual in image analysis not to have a reliable experimental setup or methodology for the right extraction of the number the particles on a cluster. In our case, we have searched for a compromise between reasonably good statistics and spatial resolution. As a result, we do not have enough image definition for detecting the individual particles inside each cluster (see Fig.1) and only the contours of the clusters have been detected.

An estimation method of Haussdorff dimension is the box-counting method consisting in covering the fractal object with boxes of different size and extracting the fractal dimension through a power law between the number of boxes and its size [42]. That is, if we cover a fractal object with a number of boxes  $N(r)$  with side  $r$ , we can obtain its capacity dimension using the following expression:

$$D_B = -\lim_{r \rightarrow 0} \frac{\log N(r)}{\log r} \quad (3)$$

This method gives the box-counting dimension or capacity dimension ( $D_B$  hereafter). Classical box-counting method presents limitations that have to be taken into account: this method is very sensitive to the resolution and orientation of the image and the power-law relationship must be verified in a reasonable range of length scales to be able to state that fractal structure appears [43]. An example can be seen on Fig. 3, where we calculate  $D_B(2D)$  for a chain during aggregation and 10 s after the field has been turned off for an experiment with  $\lambda = 703$  and  $\phi_{2D} = 0.106$ . In the first case, a capacity dimension  $D_B(2D) = 1.11 \pm 0.02$  is obtained, whereas in the second, we obtain  $D_B(2D) = 1.28 \pm 0.02$ . The range where the linear regression is fitted is almost two orders of magnitude. In Section IV, we use this method for several chains for each time and we calculate average values.

Another method for obtaining fractal dimensions from these 2D images of the projected aggregates consists on the analysis of several projected fractal dimensions using the scale relation for fractal quantities explained before. We can consider various types of these fractal dimensions: one and two dimensional fractal dimensions,  $D_1$  and  $D_2$ , which are obtained through the following form:

$$P \sim l_f^{D_1}; \quad A \sim l_f^{D_2} \quad (4)$$

where  $P$  represents the perimeter of a cluster,  $A$  the area and  $l_f$  the longest distance between two points in the cluster, the so-called Feret's diameter [34]. Another useful expression uses the area and the perimeter for obtaining the so-called perimeter-based fractal dimension  $D_p$  in the following form:

$$A \sim P^{2/D_p} \quad (5)$$

These relations let us calculate the fractal dimensions easily using 2D images captured with a digital camera. Thus, when the contour of the clusters or aggregates is detected by means of image analysis, we only need to calculate the perimeter, the area and the Feret's diameter for obtaining the corresponding 2D fractal dimension. However, some critics to the applicability of the area-perimeter method on Eq.(5) have been lately reported [44]. The main argument of that critic lies on the fact that digitalising can change the perimeter and area of the objects of study, if it is applied for objects oriented in different directions. In our case, this argument is not applicable, because of the anisotropy of the clusters caused by the external magnetic field. An example of the calculation of  $D_p$  using the area-perimeter method can be seen on Fig.4. The power law behaviour is verified in almost four orders of magnitude, showing that this method for obtaining fractal properties is adequate for a system like ours.

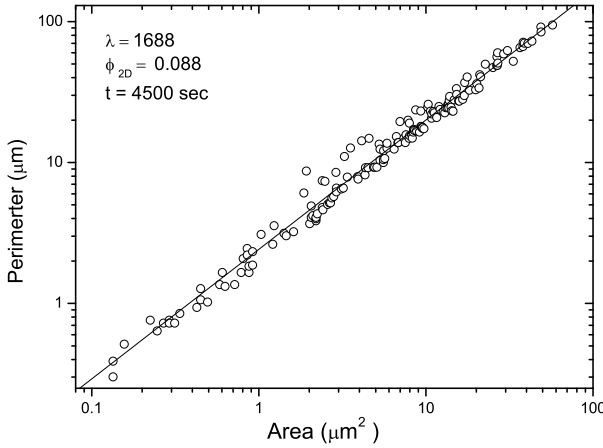


FIG. 4: Linear regression for the calculation of  $D_p$  corresponding to a magneto-rheological fluid with concentration  $\phi_{2D} = 0.088$  and  $\lambda = 1688$  after applying the magnetic field during 4500 s. A value of  $D_p = 1.84$  is obtained.

### A. Roughness.

For testing the possible interpretation of the projected fractal dimensions as a reflection of the roughness of the boundary of the clusters, we compute the height of the clusters contour measured from a central line which crosses the clusters end to end which we named as  $h_j(x, t)$ . For each cluster  $j$  in a single image, this quantity depends of the position  $x$  of the contour point and time  $t$ . For this study, we calculate the average value,  $H(t) \equiv \langle h(t) \rangle_j$ , of this height for all the clusters contained at the corresponding image. This border roughness study is different to others previously made on a single magnetic chain [45], where the fluctuations on the form of the chain were analysed, not its border.

We also calculate the border height fluctuation by means of the interface width for the cluster  $j$  as:

$$w_j(t) \equiv \sqrt{\frac{1}{N} \sum_{i=1}^N [h(i, t) - \langle h(t) \rangle_j]^2} \quad (6)$$

where  $i$  refers to the corresponding contour point and  $N$  is the total number of contour points. This quantity characterizes the roughness of the contour. We calculate a cluster average value of the border height fluctuation for each time as  $W(t) \equiv \langle w(t) \rangle_j$ . Also, we can define the height-height correlation:

$$c(l) \equiv \sqrt{[h(x) - \langle h(x') \rangle]^2} \quad (7)$$

where  $l = |x - x'|$  is the distance between two contour points projections,  $x$  and  $x'$ , made into a central end to end line that crosses the cluster. This magnitude scales in the form  $c(l) \sim l^\alpha$ , being  $\alpha$  the roughness exponent. This property has been widely used, for instance, for the study of surface growth [46] and interfacial growth phenomena by electrochemical deposition [47]. Moreover,

it is possible to connect the roughness exponent with a fractal dimension  $d$  [46]:

$$d = 2 - \alpha \quad (8)$$

Later in this work, we will show as  $D_p$ , the perimeter-based dimension, may be identified with this fractal dimension  $d$ , confirming the morphologic nature of this quantity. We also use the temporal evolution of the average height-height correlation  $W(t)$  for observing the changes on the cluster roughness during the aggregation and disaggregation processes.

## IV. RESULTS.

We calculate the capacity dimension  $D_B(2D)$  using several clusters in some images during aggregation and disaggregation. For an adequate calculation of this dimension, we extract manually well-defined and representative clusters in each image and calculate individually the box-counting dimension. Next, we make an average value of  $D_B(2D)$  for each analysed time. This method is only valid when we study objects with enough size for fitting a linear regression in an acceptable range. Besides, because of the image resolution, we cannot use this methodology in the stages in which the number of free particles is predominant. We also obtain one-dimensional ( $D_1$ ), two-dimensional ( $D_2$ ) and perimeter-based ( $D_p$ ) fractal dimensions using Eq.(4) and Eq.(5). Therefore, we fit three linear regressions in every captured image (every 0.4 sec) using our software, aiming to observe the changes on these fractal dimensions during aggregation and disaggregation. We require a regression correlation factor of at least  $r > 0.98$  for considering that the result of its respective image is correct. This condition widely reduces the number of images that are useful for this study, specially when chains are not yet formed, that is when the particles are moving free in the liquid. As it can be seen on the example in Fig. 1, we use a wide vision field for detecting as many chains as possible. This is just what happens with  $D_B(2D)$ , for small objects, like free particles, we do not have enough precision -or number of pixels- to observe clearly the particles' border, so we cannot suitably obtain their corresponding fractal dimension.

### A. Aggregation.

As it has been commented in the Introduction, a few studies about fractal dimension of aggregates using magnetic particles have been developed in the last two decades. The differences between experimental systems imply that a complicated issue can arise from the comparison between different obtained fractal dimensions. However, it is obtained that all the values relating chain-like structures of magnetic particles for three-

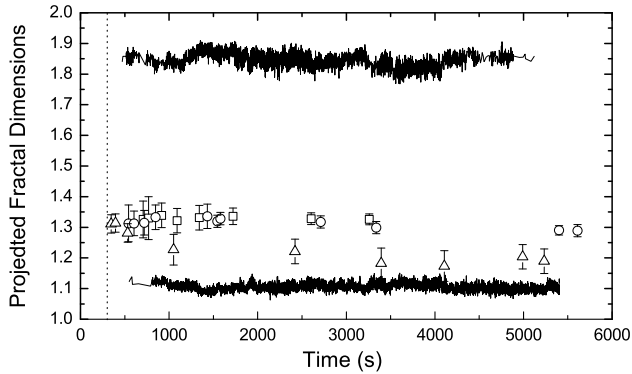


FIG. 5: Temporal evolution of projected projected fractal dimensions during aggregation. Continuous lines  $D_2$  (bottom) and  $D_p$  (top) for a case of  $\lambda = 703$  and  $\phi_{2D} = 0.106$  (correlation factor  $r > 0.98$ ). The single points represent box-counting dimension  $D_B(2D)$ :  $\lambda = 131$  and  $\phi_{2D} = 0.071$  for squares;  $\lambda = 176$  and  $\phi_{2D} = 0.115$  for circles;  $\lambda = 703$  and  $\phi_{2D} = 0.106$  for triangles.

dimensional fractal dimensions are contained in a interval  $D_f = 1.1 - 1.3$ . For instance, using light scattering, it is possible to obtain  $D_f$  adjusting the scattering intensity  $I$  with the scattering vector  $q$  between the Guinier and the Porod regimes, where is verified  $I \propto q^{-D_f}$  [15]. Various works can be found on the literature which use light scattering: spherical vesicles containing magnetic particles (magnetic liposomes) which gives a value of  $D_f = 1.1 \pm 0.1$  [28], organic-solvent-based magnetic fluids compressing disperse magnetite nanoparticles with  $D_f = 1.22$  [27], and magneto-rheological fluids with  $D_f = 1.21 \pm 0.14$  [25] and  $D_f = 1.24 \pm 0.04$  [26]. By means of the expressions explained in last section, it may be possible to compare perimeter-based fractal dimension with three-dimensional fractal dimensions obtained using light scattering [34]. Helgesen *et al* [21] reported variation of fractal dimension with the magnetic strength for a 2D system of  $3.6 \mu\text{m}$  magnetic particles contained in a cell of  $5 \mu\text{m}$  thickness. The fractal dimension is calculated using video-microscopy and Ec.(2). In fact, their obtained fractal dimension must not be considered three-dimensional but two-dimensional, because of their experimental system is clearly two-dimensional. The magnetic interaction is measured using the factor  $K_{dd} = m^2/8a^3k_B T$ . Comparing this quantity with our equivalent  $\lambda$  factor, we obtain  $K_{dd} = \lambda/2$  using S.I. units. In their study, magnetic particles have a permanent magnetic moment, thus comparison between our experiments and theirs is complicated. In one case, they apply a external magnetic field of  $H = 1$  Oe, generating chains aligned with the external field. This experiment, the more compatible with ours, a value of  $D_2 = 1.05 \pm 0.03$  for  $K_{dd} = 1360$  ( $\lambda = 680$ ) is obtained. Simulations have been reported on magnetic fluids including van der Waals, electrostatic, magnetic dipole and hydrodynamic inter-particle forces [32]. In that work, Chin *et al* obtain values for fractal dimension inside the interval  $D_f = 1.1 - 1.3$  for magnetic

fields 0.1, 1 and 2 T. However, tangential magnetic dipole forces have not been included, so aggregates do not have a chain structure, nor are aligned with the magnetic field and therefore comparison with real experimental systems may be not applicable. Changes and temporal evolution of fractal dimension during aggregation have been studied on latex micro-spheres [14], and lately on magneto-rheological fluids [26].

In Fig. 5, we display an example of the values of  $D_2$  and  $D_p$  obtained along the aggregation process with the requirement of  $r > 0.98$ . We also represent several average values of  $D_B(2D)$  for three different experiments. A temporal dependence in projected fractal dimensions is not detected and a relatively uniform value for fractal dimensions which do not depend of aggregation dynamics is found, i.e., the fractal dimension is constant in time, although dynamical quantities such as number of clusters, mean cluster size and others similar magnitudes follow a power law behaviour in this kind of systems [40, 48]. We do not observe temporal variation of these fractal dimensions during initial stages of aggregation. This is because free particles are not detected suitably and this reduce considerably the correlation factor on linear regressions. As we justify later in this work, we can interpret capacity dimension as a measure of the degree of cluster space filling, while the perimeter-based dimension is linked with the clusters border roughness. When clusters become linear chains, these kind of aggregates do not change the way they fill the space (they are almost linear objects) and the box counting dimension do not vary. In the same way, chains' border roughness does not suffer special alterations during aggregation and consequently  $D_p$  does not show any variation.

We calculate the projected fractal dimensions varying  $\lambda$  and  $\phi_{2D}$ . The obtained values for  $D_2$  and  $D_p$  are summarized on Table I on columns 3 and 4, the associated  $\lambda$  and  $\phi_{2D}$  values can be consulted on columns 1 and 2. No dependency with  $\lambda$ ,  $\phi_{2D}$  or with the ratio  $R_1/R_0$  is observed on these fractal dimensions. Therefore, we assume that making average values using all the experiments is a correct procedure. We also calculate the one dimensional dimension  $D_1$  for the chains, also with no variation or dependencies during aggregation, obtaining an average value of  $\langle D_1 \rangle = 1.01 \pm 0.03$ . One-dimensional fractal dimension gives some information about the irregularity on the perimeter of the aggregate. For Euclidean dimension, we must have  $D_1 = 1$ . In our case, we obtain a very similar value to this Euclidean result, probably because of the linear and field-aligned structure of the chains. Perhaps, as proposed Lee *et al* [34], could be argued the existence of a relation among circularity  $C$  and  $D_1$ , since  $C$  also measures the aggregate morphology as  $D_1$  does. Nevertheless, no correlation is observed between  $D_1$  and  $C$  for different kind of clusters, as Lee *et al* obtained. In our case, where aggregates are linear chains,  $C$  varies in the aggregation process with a power law behavior during aggregation (as it can be seen on Fig. 2), while  $D_1$  keeps constant.

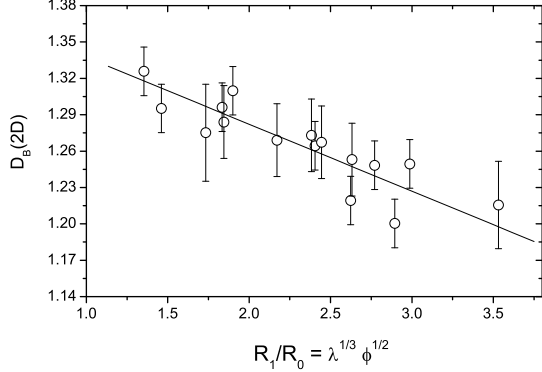


FIG. 6: Dependency of  $D_B(2D)$  with the ratio  $R_1/R_0$  during aggregation (Table I, columns 6 and 3). The continuous line represent a linear regression of the experimental data giving  $D_B(2D) = (-0.06 \pm 0.01)R_1/R_0 + (1.39 \pm 0.02)$  with a correlation factor  $r = -0.873$ .

Two-dimensional fractal dimensions  $D_2$  and  $D_p$  are more useful than one-dimensional fractal dimension  $D_1$  in terms of characterizing the formed chains from our magneto-rheological system. These dimensions not only give information about the morphology of the aggregates, but they also supply mechanical strength information about the aggregate. For two-dimensional fractal dimension  $D_2$ , an average value of  $\langle D_2 \rangle = 1.09 \pm 0.02$  is obtained. This value is quite close to the expected  $D_2 = 1$  for a linear object in an Euclidean geometry and is compatible with the previous value obtained by Helgesen *et al* of  $D_2 = 1.05 \pm 0.03$ . For the perimeter-based dimension  $D_p$ , we obtain an average value of  $\langle D_p \rangle = 1.84 \pm 0.02$ . Both values,  $D_2$  and  $D_p$ , must be in an interval between 1 and 2. For  $D_p = 1$ , we have a perfect spherical object, whereas for  $D_p = 2$ , we obtain a linear object. In our case, we obtain a value close to 2, so the aggregates are linear objects. The main practical difference among  $D_2$  and  $D_p$  is that  $D_p$  is obtained from magnitudes which are calculated more directly (area and perimeter) and that  $D_2$  (and  $D_1$ ) is calculated by means of Feret's diameter, i.e.,  $D_p$  reflects better the roughness of the boundary of the aggregate. For this reason, a value for  $D_p$  is obtained not so close to 2 than  $D_2$  to 1.

In contrast to  $D_1$ ,  $D_2$  and  $D_p$ , the capacity dimension seems to show a relation with the external parameters, so an average value cannot be calculated. In fact, we find a linear dependence with the ratio  $R_1/R_0$  as can be seen on Fig. 6. As we mentioned on the Introduction, the ratio  $R_1/R_0$  informs about whether the chains initially aggregate by magnetic interaction ( $R_1 > R_0$ ) or by diffusion ( $R_1 < R_0$ ). In all our experiments  $R_1/R_0 > 1$  is verified, therefore, from the beginning, the aggregation process is dominated by the magnetic interaction among particles. Moreover, this result shows that the shape of the chains depends on the intensity of this ratio. Visually, we observe that the finer and longer formed chains at the stationary state correspond to higher values of the

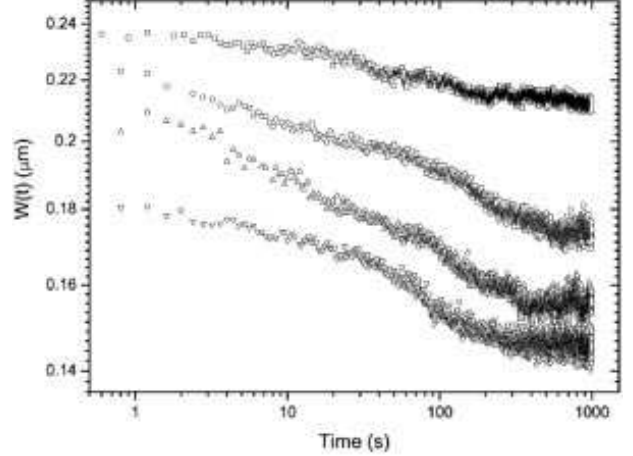


FIG. 7: Four experiments as examples of power-law behaviour of the average chain-border height fluctuation  $W(t)$  in the initial stages of aggregation ( $t < 100$  s) until saturation. From top to bottom:  $\lambda = 131$  and  $\phi_{2D} = 0.071$ ;  $\lambda = 703$  and  $\phi_{2D} = 0.106$ ;  $\lambda = 252$  and  $\phi_{2D} = 0.145$ ;  $\lambda = 1688$  and  $\phi_{2D} = 0.088$ .

ratio  $R_1/R_0$ , while wider chains are observed when the ratio is lower. Therefore, the shape of the clusters may depend of the intensity of this magnetic interaction between particles. This implies that the capacity dimension measures how the chains fill the surrounding space.

In the Introduction, we introduced various concepts related with the roughness to the clusters contour, in particular, the border height fluctuation  $W(t)$ . For our experiments, we observe that  $W(t)$  is approximately constant during aggregation from 100 s, until the field is switched off (see Fig. 7). In Table I, column 7, we show time average values  $\langle W \rangle_t$  for each experiment in the saturated region. No dependence with  $\lambda$ ,  $\phi_{2D}$  or  $R_1/R_0$  is observed. Therefore, as it happens with  $D_p$ , the variations on the border of the clusters do not suffer high variations during aggregation and they seem not to depend on external variables, with the exception of the initial stages of aggregation. The average value of this dispersion is  $0.21 \pm 0.04 \mu\text{m}$ , approximately 1/5 of the particle diameter. This value can be considered high for linear chains, because a perfect spherical single particle should have a value of  $w$  close to 1/3 of the particle diameter. However, the quantities  $\langle W \rangle_t$  have been obtained making a cluster average in which the free particles and small chains count the same as the longest clusters. Similarly, the initial value when no field is applied may vary as a function of the number of initial aggregates present in the system. Therefore, this average and experimental variations for ideal scenarios may reduce the value of  $W(t)$  for a perfect chain composed of aligned spherical particles. We observe as the average chain-border height fluctuation  $W(t)$  follows a power-law behaviour on the initial stages of aggregation, as can be seen for various experiments on Fig. 7. Consequently, we define the exponent  $\beta_a$ , so during initial stages  $W(t) \sim t^{\beta_a}$  is verified. We summarize



FIG. 8: Example of chains disaggregating for different times in the experiment  $\lambda = 131$  and  $\phi_{2D} = 0.071$ . The contour around the chains is the border of the clusters detected by means of the image analysis, while the grey color is the original captured image. Left:  $t = 0$  s (when field is off), Middle:  $t = 20$  s, and Right:  $t = 40$  s

$\beta_a$  obtained values on Table I on column 5. An average value for this exponent is  $\langle \beta_a \rangle = -0.03 \pm 0.02$ . The high relative error of this magnitude is associated with the differences in number and morphology between the detected clusters in each experiment, specially regarding the free particles.

In addition, and as a verification, we calculated the roughness factor  $\alpha$  for chains with sufficient length. We obtain a average value of three aligned chains ( $\sim 20 \mu\text{m}$  length)  $\alpha = 0.11$  in a case of  $\lambda = 703$  and  $\phi_{2D} = 0.106$  and for different times  $t = 4105.6$  s,  $5233.2$  s and  $5400$  s. If we apply Ec.(8), we obtain an average value of  $d = 1.88 \pm 0.03$ , compatible with the value  $D_p = 1.85$  obtained for this experiment and with the average  $\langle D_p \rangle = 1.84 \pm 0.02$ . As we will see below, this method also gives, where it is applicable, concordance between  $d$  and  $D_p$  in the disaggregation process. Therefore, we can interpreter perimeter-based fractal dimension as a measure of the roughness of the chains border.

At this point we would like to compare our experimental findings with previous results on magneto-rheological fluids using light scattering. However this comparison may not be possible because of the nature of the three-dimensional fractal dimension obtained by static light scattering and the fractal dimension obtained using projected images as in our experiments. However, theoretical expressions showed in the Appendix has been developed to carried out such a comparison. An adequate knowledge on this subject would be interesting in colloids for understanding the dynamics of the aggregates and their morphological evolution. Therefore, with our results of  $D_2$ , we obtain an average value of  $\langle D_f \rangle = 1.419 \pm 0.002$  using Ec.(A1a). By means of Ec.(A1b), we obtain an average value  $\langle D_f \rangle = 1.58 \pm 0.04$ . Both results seem to give overestimated values, taking into account that they are clearly linear aggregates, especially regarding Ec.(A1b). Using the linear regression result Ec.(A2) on the data from Sánchez *et al.*, a more sounder value is obtained. An average gives  $\langle D_f \rangle = 1.28 \pm 0.04$ . A result quite close to this average is obtained by means of Ec.(A3), using a resolution of  $N_{pix} = 1072$  px, a similar resolution to our experimental system. Therefore, we obtain an average three-dimensional capacity dimension of

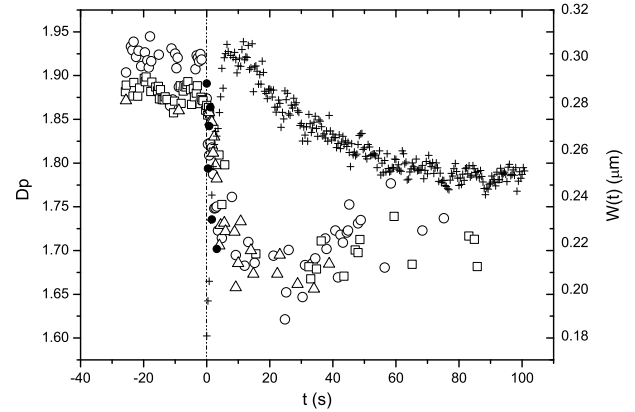


FIG. 9:  $D_p$  during disaggregation when the field is switched off ( $t = 0$ ) in three different experiments (circles:  $\lambda = 131$  and  $\phi_{2D} = 0.071$ ; squares:  $\lambda = 176$  and  $\phi_{2D} = 0.068$  and triangles:  $\lambda = 703$  and  $\phi_{2D} = 0.106$ ). The little crosses correspond to the average chain-border height fluctuation  $W(t)$ . The black filled points are  $d = 2 - \alpha$  values for the experiment  $\lambda = 703$  and  $\phi_{2D} = 0.106$

$\langle D_B(3D) \rangle = 1.34 \pm 0.01$ . Then, the more similar value that we have obtained comparing with previous experiments using static light scattering, is  $\langle D_f \rangle = 1.28 \pm 0.04$ , by means of the linear regression fitted with the data by Sánchez *et al.* Ec.(A2). A little higher value is obtained with the average value for the capacity dimension  $D_B(3D)$ , using Ec.(A3), this may be because the box-counting method gives imprecise results, due to its dependency of the pixel resolution.

## B. Disaggregation.

As it has been said before, it is difficult to obtain reliable results on fractal dimensions, when we have free particles because of image resolution. That is why we cannot observe the variation on fractal dimensions while the chains are being formed by the aggregation of individual particles. However, we can observe the disaggregation process, i.e, the separation by Brownian motion and repulsive electrostatic forces of the particles that formed the chains when the applied field is switched off. Surprisingly, in the literature, this kind of processes have rarely been studied [49, 50]. Developed studies focus on aggregation, but not on the process of the aggregates that vanish and become free particles. This is very interesting for practical applications, for example, for designing an on-off dispositive based on magneto-rheological fluids. In Fig. 9, we show three snapshots of a group of chains during disaggregation at times  $t = 0$  (field is turned off),  $t = 20$  s and  $t = 40$  s. The dark border along the clusters border is the contour extracted using our software. It can be seen how the free particles have appeared at 20 seconds and how the clusters contour turns into itself.

The evolution of  $D_p$  in the disaggregation process for

three different experiments varying  $\lambda$  and  $\phi_{2D}$  values is displayed on Fig. 9. The perimeter-based fractal dimension  $D_p$  changes from the value  $D_p \sim 1.90$  for linear chains to a minimum value  $D_p \sim 1.65$  after 20 seconds of Brownian motion. After that, a stabilization on  $D_p$  (for  $t > 40$  s) is observed. We have to say that this method presents several limitations at this point: first, the presence of free particles reduces the correlation factor of the linear regression, making the result less reliable. Second, as it has been commented in the Introduction, this method could not be correct when the objects do not present anisotropy, as occurs when the chain disaggregates into free particles. Therefore,  $D_p$  values may not be correct when  $t > 60$  s during disaggregation.

In Fig. 9, we also represent (little crosses) the evolution of the average chain-border height fluctuation  $W(t)$ . Two separated states can be observed on this magnitude: the first, an steep growth from  $t = 0$  until  $t \sim 10$  s; the second, a soft decrease of the curve until saturation. Both behaviours present, separately, power-law behaviours with, of course, different exponents. We respectively named these exponents as  $\beta_{d1}$  and  $\beta_{d2}$  and their values for each experiment have been summarized on Table I columns 9 and 10. Average calculations of both quantities give the following results:  $\langle \beta_{d1} \rangle = 0.15 \pm 0.06$  and  $\langle \beta_{d2} \rangle = -0.11 \pm 0.03$ . We interpret these two regions as follows: the first region represents the region where the rugosity of the clusters grows because of the simple movement of the particles inside the cluster. In this stage, the clusters maintain their individuality not breaking yet into little pieces. This behaviour means univocality in the contour points. The second region appears when the clusters begin to break into little clusters and the free particles appear. At this point the growth on the average cluster rugosity decreases, because the average is calculated with the new clusters and free particles that appear during the process. A crucial point for calculating the roughness exponent  $\alpha$  in our clusters using the height-height correlation function Eq.(7) is the univocality of the contour. That means that, each  $x$  point must be associated to one and only one height. When the disaggregation process is advanced and the free particles appear, the detected contour becomes not univocal and tends to twist itself up. When this behaviour occurs, it is not possible to use this method. For this reason, we observe that we can only calculate  $\alpha$  values for  $t < 4$  s. In Fig. 9, using black filled points, we plot some calculations of  $d = 2 - \alpha$  (Eq.(8)) for a long chain in an experiment with  $\lambda = 703$  and  $\phi_{2D} = 0.106$ . The points of  $d$  fit adequately to the represented  $D_p$  points and values seem to be very similar. For that reason, we conclude that the perimeter-based dimension,  $D_p$ , is a measure related with the rugosity of the clusters contour.

Finally, we calculate some average values for the box-counting dimension during disaggregation. These calculations can be seen on Fig. 10. As we see on the study of aggregation, the box-counting dimension is different for each experiment depending on the ratio  $R_1/R_0$ , therefore

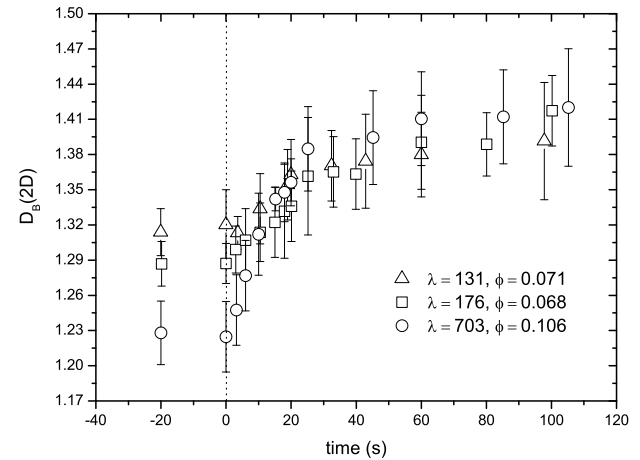


FIG. 10: Box-counting dimension during disaggregation for three different experiments. Each case begins the process with different  $D_B(2D)$  values, but the fractal dimension tends to a common temporal evolution while the chains lose its linear structure.

the experiments begin the disaggregation process with different values of  $D_B(2D)$ . However, when the field is switched off, all the values tend to a single curve. This might be the expected behaviour, if we suppose that the capacity dimension measures how the clusters occupy the space, since the clusters tend to dissolve into little clusters and particles, regardless of the characteristics of the field and concentration at beginning of the aggregation process.

## V. CONCLUSIONS.

In this work, we study experimentally the cluster morphology in a magneto-rheological fluid (MRF) under a constant uniaxial magnetic field. We calculate 2D fractal dimensions and study the contour roughness of the cluster using image analysis. We study two processes: the aggregation, where the rod-like chains formed by the application of the external magnetic field, and the disaggregation which occurs when the magnetic field is switched off. As far as we know, the disaggregation process has not been studied in detail in the literature, in spite of its interest on potential practical applications.

During aggregation, we do not observe any regular temporal variation on fractal dimensions, because the method used in this work cannot be applied to the initial stages of aggregation. Using the area-perimeter method, we obtain the following average values for: one-dimensional fractal dimension,  $\langle D_1 \rangle = 1.01 \pm 0.03$ ; two-dimensional fractal dimension,  $\langle D_2 \rangle = 1.09 \pm 0.02$  and perimeter-based fractal dimension,  $\langle D_p \rangle = 1.84 \pm 0.02$ . We compare these values with previous experimental works. We show that the fractal dimension obtained by Helgesen *et al* [21] is indeed a two-dimensional fractal dimension. We obtain a good agreement between their

TABLE I: 2D fractal dimensions and  $\beta$  exponents. (Units for  $\langle W \rangle_t$  are  $\mu\text{m}$ .)

$\lambda$	$\phi_{2D}$	$R_1/R_0$	$D_2$	$D_p$	$D_B^{2D}$	$\langle W \rangle_t$	$\beta_a$	$\beta_{d1}$	$\beta_{d2}$
131	0.071	1.34	1.14	1.85	1.33	0.21	-0.02	0.23	-0.16
131	0.132	1.85	1.03	1.89	1.28	0.17	-0.04	0.19	-0.11
176	0.068	1.46	1.09	1.89	1.30	0.20	-0.03	0.14	-0.15
176	0.115	1.90	1.10	1.84	1.31	0.17	-0.03	0.17	-0.10
252	0.145	2.41	1.07	1.84	1.26	0.16	-0.05	0.15	-0.09
390	0.112	2.45	1.1	1.87	1.27	0.19	-0.03	0.17	-0.09
536	0.051	1.83	1.10	1.82	1.30	0.22	-0.02	0.16	-0.13
536	0.086	2.38	1.05	1.92	1.27	0.18	-0.03	0.20	-0.12
703	0.038	2.41	1.11	1.84	1.28	0.21	-0.02	0.10	-0.07
703	0.106	2.90	1.10	1.85	1.20	0.20	-0.04	0.15	-0.13
888	0.051	2.17	1.05	1.87	1.27	0.25	-0.01	0.06	-0.12
888	0.075	2.63	1.05	1.85	1.25	0.26	-0.02	0.19	-0.08
1485	0.059	2.77	1.08	1.84	1.25	0.22	-0.05	0.03	-0.12
1688	0.088	3.53	1.10	1.87	1.22	0.15	-0.05	0.21	-0.09
1891	0.045	2.62	1.09	1.82	1.22	0.22	-0.06	0.21	-0.15
2989	0.043	2.99	1.07	1.78	1.25	0.3	-0.01	0.07	-0.14

value with a external applied field ( $D_2 = 1.05 \pm 0.03$ ) and our result for two-dimensional fractal dimension. We obtain that the box-counting dimension or capacity dimension  $D_B(2D)$  does not vary with time, but its value is different depending on the ratio  $R_1/R_0$  between two characteristic lengths that measures a relative magnetic field strength for particle. We also calculate various quantities associated with the roughness of the contour or border of the clusters. We find that the average chain-border height fluctuation  $W(t)$  follows a power-law exponent, in the initial stages of the aggregation process, with an average exponent  $\langle \beta_a \rangle = -0.03 \pm 0.02$ .

During the process of chain disaggregation, i.e., when the applied field is switched off and the chains vanish because of the Brownian motion and electrostatic repulsive forces, we observe that  $D_p$  decreases approximately a 13% factor when the field is switched off. Also, we show that  $W(t)$  presents two different power-law behaviours with exponents  $\langle \beta_{d1} \rangle = 0.15 \pm 0.06$  and  $\langle \beta_{d2} \rangle = -0.11 \pm 0.03$ . Moreover, we show that the perimeter-based dimension is related with the fractal dimension  $d$  obtained directly by means of the roughness exponent  $\alpha$  in Eq.(8). This means that we may interpret the perimeter-based dimension as a measure of the clusters border roughness. Finally, we show results on the evolution of box-counting dimension during disaggregation. The differences among experiments on this fractal dimension vanish as the clusters dissolve. This behaviour fits with an interpretation of  $D_B(2D)$  as a measure of how the clusters fill the space.

In conclusion, for a better understanding of temporal evolution and dependencies of fractal dimension in MRF and for confirming the results hereby exposed, it would be necessary to carry out more investigations. Specifically, simulations of MRF could be implemented using a 3D system with a real set of interactions including electrostatic, van der Waals, Brownian motion and complete

magnetic dipole forces. Such a model could be quite useful for an adequate study of fractal dimensions and for a better knowledge of the relation between three-dimensional fractal dimension and projected fractal dimensions at an anisotropic colloidal system like the used in this work. Moreover, we will focus further investigations on temporal evolution of aggregates' box-counting and correlation dimension and its dependence with magnetic strength and concentration for the initial stages of aggregation.

## VI. ACKNOWLEDGMENTS.

We wish to acknowledge N. Sánchez for providing us with explicit data from his work, as well as his comments; ICMM researchers at CSIC for the VSM magnetometry measurements and J. C. Gómez-Sáez for her correction of the English version of this manuscript. P. Domínguez-García has been supported by a F.P.I. fellowship from M.E.C. This research has been supported by M.E.C. under Project No. BFM2001-0297.

## APPENDIX A: CALCULATING THREE-DIMENSIONAL FRACTAL DIMENSION.

How the values of these 3D and 2D-projected fractal dimensions relate to each other is not an straightforward matter. As we explained before,  $D_f$  is usually obtained directly by means of light scattering, which is a very effective experimental method in the study of colloidal suspensions. However, it would be very useful to obtain this three-dimensional fractal dimension using image analysis techniques. Some elaborated techniques have been developed regarding this problem, for instance, the two-slopes dimensional analysis using cumulative size distribution [51] or the relative optical density method [52]. The main question at this point is how to correlate easily these 2D projected fractal dimensions with the magnitude which is actually useful physically: the three dimensional fractal dimension  $D_f$ . A possible answer could be that  $D_{proj} = \min\{2, D_f\}$  [1], but this result has been obtained for mathematical infinite self-similarity fractal objects and might not be applicable for real finite fractals, such as aggregates. A mathematical approach to this argument can be consulted on [35]. Some theoretical studies have been developed in the last years to explore the possibility of obtaining  $D_f$  using the projected fractal dimensions. In these works, the authors attempt to find a relation between the three-dimensional fractal dimension and the projected ones, using simulations of aggregation of particles in a three dimensional space. Afterwards, they calculate  $D_f$  and the projected dimension and try to find mathematical relations between them. An initial work of the above-mentioned corresponds to Jullien *et al* [53], but their results may be not applicable to real

fractal aggregates [35]. As far as we know, the most important approaches to this question appear in the works by Lee and Kramer [34], Maggi and Winterwerp [35] and Sánchez *et al* [36]. In the first above-mentioned works, Lee and Kramer find the following expressions between  $D_f$  with  $D_2$  and  $D_p$  [54]:

$$D_f = 1.391 + 0.01e^{2.164D_2} \quad (\text{A1a})$$

$$D_f = -1.628D_p + 4.6 \quad (\text{A1b})$$

Although these two expressions are praiseworthy, the regression coefficient for Ec. (A1b) should be higher than the obtained  $r = 0.83$ , concluding that a reliable value of  $D_f$  by means of the projected dimension  $D_p$  has been demonstrated. Moreover, Ec. (A1b) must verify the boundary conditions for  $D_f$  and  $D_p$ , i.e., for a spherical object,  $D_p = 1$  and  $D_f = 3$ , and for a linear object,  $D_p = 2$  and  $D_f = 1$ . The first boundary condition is approximately verified, but not the second. On the other hand, Ec. (A1a), which correlates  $D_f$  with  $D_2$ , has a higher correlation factor ( $r = 0.96$ ) and seems to be more reliable.

The boundary conditions for  $D_f$  and  $D_p$  suggest a possible approximate linear expression in the form  $D_f \simeq -2D_p + 5$ , which is approximately obtained using the data provided by Sánchez *et al* from their astrophysical-related work. In their study, Sánchez *et al* calculate a relation between  $D_p$  and  $D_f$  using simulations of random aggregates aiming to obtain the fractal dimension of interstellar molecular clouds by analysing the projected images of these objects. They gather that these relations mostly depend on the image resolution  $N_{pix}$ , especially at low values of  $D_p$  ( $1 < D_p < 1.6$ ). However, as it can be seen on their work, there is an intermediate zone where there is no apparent dependence on the image resolution for values of  $D_p$  contained in the interval  $1.6 < D_p < 1.9$ . For these data, a linear regression can be calculated, obtaining the following expression:

$$D_f = (-2.09 \pm 0.13)D_p + (5.15 \pm 0.22); \quad (\text{A2})$$

for  $1.6 < D_p < 1.9$

The Ec.(A2) verifies the two above-mentioned boundary

conditions between  $D_f$  and  $D_p$  and gives an interval of application independent to the resolution. A mathematical approach for obtaining the three-dimensional capacity dimension  $D_B(3D)$ , from two-dimensional projections of fractal aggregates is present in the work by Maggi and Winterwerp [35]. For statistical self-similar and non-homogeneous fractals, as fractal aggregates, it is usual to study the generalized dimension of  $q$ th order,  $d_q$  [55]. The fractal dimension associated with  $q = 0$  gives  $d_0$ , being this dimension the capacity dimension  $D_B$ . Maggi and Winterwerp apply the current theory of projections of fractals for obtaining the three-dimensional capacity dimension,  $D_B(3D)$ , that depends on perimeter-based dimension in the following form:

$$D_B(3D) = \sqrt{\frac{a(N_{pix})}{D_p - b(N_{pix})}}; \quad \text{for } D_p < 2 \quad (\text{A3})$$

where  $a(N_{pix})$  and  $b(N_{pix})$  are functions of the resolution  $N_{pix}$ . In the case of infinite resolution  $l \rightarrow \infty$ ,  $a = 9/8$  and  $b = 7/8$  is obtained. Therefore, it is possible to apply Ec.(A3) with the image resolution of our experiment. For example, for a resolution of  $N_{pix} = 1024$  px,  $a = 1.483$  and  $b = 1.035$  are obtained. An important result deduced of this study is that it is not possible to obtain three-dimensional information from the two-dimensional capacity dimension  $D_B(2D)$ . This result limits the utility of the box-counting fractal dimension for being compared with another similar quantities. In previous sections, we explained our results for the calculation of 2D projected fractal dimensions by means of image analysis. Afterwards, we calculated and compared the three-dimensional fractal dimensions obtained by the formed chains using the expressions explained in this section. The result that seems to be more simple and applicable to our system is the obtained by Sanchez *et al* [36] which provide an approximate linear expression in the form  $D_p \simeq -2D_p + 5$  on the range of  $1.6 < D_p < 1.9$  and which is independent of image resolution. This result provides a value for three-dimensional fractal dimension of  $\langle D_f \rangle = 1.28 \pm 0.04$ , compatible with light scattering studies of similar frameworks on MRF [25, 26].

---

[1] B. Mandelbrot, *The Fractal Geometry of Nature* (W. H. Freeman and Co., San Francisco, 1982).

[2] J. Feder, *Fractals* (Plenum press, New York, 1988).

[3] M. Keipes, F. Ries, and M. Dicato, *Biomed. Pharmacother.* **47**, 409 (1993).

[4] A. Brú, J. M. Pastor, I. Fernaud, I. Brú, S. Melle, and C. Berenguer, *Phys. Rev. Lett.* **81** (**18**), 4008 (1998).

[5] G. Murante, A. Provenzale, E. A. Spiegel, and R. Thieberger, *Ann. N. Y. Acad. Sci.* **867**, 258 (1998).

[6] M. Tirado-Miranda, A. Schmitt, J. Callejas-Fernández, and A. Fernández-Barbero, *J. Chem. Phys.* **119** (**17**), 9251 (2003).

[7] G. Odriozola, R. Leone, A. Schmitt, J. Callejas-Fernández, R. Martínez-García, and R. Hidalgo-Álvarez, *J. Chem. Phys.* **121** (**11**), 5468 (2004).

[8] M. Tirado-Miranda, M. A. Rodríguez-Valverde, A. Schmitt, J. Callejas-Fernández, and A. Fernández-Barbero, *Colloids Surf., A* **270** **271**, 309 (2005).

[9] A. E. González, G. Odriozola, and R. Leone, *Europhys. J. E. Soft. Matter.* **13**, 165 (2004).

[10] C. Allain, M. Cloitre, and F. Parisse, *J. Colloid Interface Sci.* **178**, 411 (1996).

[11] C. Johnson, X. Li, and B. Logan, *Environ. Sci. Tech.* **30**, 1911 (1996).

- [12] F. Gruy and P. Cugniet, *J. Colloid Interface Sci.* **272**, 465471 (2004).
- [13] J. S. Chen, T. Moschakis, and L. A. Pugnaloni, *Food Hydrocolloids* **20** (4), 468 (2006).
- [14] R. K. Chakraborti, K. H. Gardner, J. F. Atkinson, and J. E. V. Benschoten, *Water Res.* **37**, 873 (2003).
- [15] G. C. Bushell, Y. D. Yan, D. Woodfield, J. Raper, and R. Amal, *Adv. Colloid Interface Sci.* **95**, 1 (2002).
- [16] J. C. Crocker and D. G. Grier, *J. Colloid Interface Sci.* **179**, 298 (1996).
- [17] M. Fermigier and A. P. Gast, *J. Colloid Interface Sci.* **154**, 522 (1992).
- [18] J. Promislow, A. P. Gast, and M. Fermigier, *J. Chem. Phys.* **102**, 5492 (1994).
- [19] S. Melle, M. A. Rubio, and G. G. Fuller, *Phys. Rev. Lett.* **87**, 115501 (1 (2001).
- [20] S. Melle, M. A. Rubio, and G. G. Fuller, *Int. J. Modern Phys. B* **15** (6-7), 758 (2001).
- [21] G. Helgesen, A. T. Skjeltorp, P. M. Mors, R. Botet, and R. Jullien, *Phys. Rev. Lett.* **61**, 1736 (1988).
- [22] J. R. Ding and B. X. Liu, *Phys. Rev. B* **40**, 1736 (1989).
- [23] G. A. Niklasson, A. Torebring, C. Larsson, C. G. Granqvist, and T. Farestam, *Phys. Rev. Lett.* **60**, 1735 (1988).
- [24] J. L. Carrillo, F. Donado, and M. E. Mendoza, *Phys. Rev. E* **68**, 061509 (1 (2003).
- [25] F. Martínez-Pedrero, M. Tirado-Miranda, A. Schmitt, and J. Callejas-Fernández, *Colloids Surf., A* **270-271**, 317 (2005).
- [26] F. Martínez-Pedrero, M. Tirado-Miranda, A. Schmitt, and J. Callejas-Fernández, *J. Chem. Phys.* **125**, 084706 (2006).
- [27] L. Shen, A. Stachowiak, S. E. K. Fateen, P. E. Laibinis, and T. A. Hatton, *Langmuir* **17**, 288 (2001).
- [28] P. Licinio and F. Frézard, *Braz. J. Phys.* **31** (3), 356 (2001).
- [29] T. Vicsek, *Fractal Growth Phenomena*. (World Scientific, Singapore, 1992), 2nd ed.
- [30] R. Jullien and R. Botet, *Aggregation and Fractal Aggregates* (World Scientific, Singapore, 1987), 2nd ed.
- [31] R. Pastor-Satorras and J. M. Rubí, *J. Magn. Magn. Mater.* **221**, 124 (2000).
- [32] C. J. Chin, S. C. Lu, S. Yiacoumi, and C. Tsouris, *Sep. Sci. Technol.* **39** (12), 2839 2862 (2004).
- [33] P. H. Coleman and L. Pietronero, *Phys. Rep.* **213**, 311 (1992).
- [34] C. Lee and T. A. Kramer, *Adv. Colloid Interface Sci.* **112**, 49 (2004).
- [35] F. Maggi and J. C. Winterwerp, *Phys. Rev. E* **69** (2004).
- [36] N. Sánchez, E. J. Alfaro, and E. Pérez, *Astrophys. J.* **625**, 849 (2005).
- [37] L. P. Faucheuix and A. J. Libchaber, *Phys. Rev. E* **49**, 5158 (1994).
- [38] S. Melle, O. G. Calderon, M. A. Rubio, and G. G. Fuller, *J. Non-Newtonian Fluid Mech.* **102**, 135 (2002).
- [39] ImageJ, U. S. National Institutes of Health, Bethesda, Maryland, USA, URL <http://rsb.info.nih.gov/ij/>.
- [40] T. Vicsek and F. Family, *Phys. Rev. Lett.* **52**, 19, 1669 (1984).
- [41] P. Gwaze, O. Schmid, H. J. Annegarn, M. O. Andreae, J. Huth, and G. Helas, *J. Aerosol Sci.* **37**, 820 (2006).
- [42] T. G. Smith, G. D. Lange, and W. B. Marks, *J. Neurosci. Meth.* **69**, 123 (1996).
- [43] J. M. Halley, S. Hartley, A. S. Kallimanis, W. E. Kunin, J. J. Lennon, and S. P. Sgardelis, *Ecolog. Lett.* **7**, 254 (2004).
- [44] A. R. Imre, *Appl. Math. Comp.* **173**, 443 (2006).
- [45] A. S. Silva, R. Bond, F. Plouraboué, and D. Wirtz, *Phys. Rev. E* **54** (1996).
- [46] A.-L. Barabsi and H. E. Stanley, *Fractal concepts in surface growth* (Cambridge University Press, 1995), 2nd ed.
- [47] J. M. Pastor and M. A. Rubio, *Phys. Rev. Lett.* **76**, 1848 (1996).
- [48] P. Domínguez-García, S. Melle, J. M. Pastor, and M. A. Rubio (2007), (to be published).
- [49] C. J. Chin, S. Yiacoumi, and C. Tsouris, *Colloids Surf., A* **204**, 63 (2002).
- [50] S. Melle, Ph.D. thesis, Universidad Nacional de Educación a Distancia. (2002).
- [51] S. Tang, Y. Ma, and I. M. Sebastian, *Colloids Surf., B* **20**, 211 (2001).
- [52] K. Tian, K. A. Thomson, F. Liu, D. R. Snelling, G. J. Smallwood, and D. Wang, *Combust. Flame* **144**, 782 (2006).
- [53] R. Jullien, R. Thouy, and F. Ehrburger-Dolle, *Phys. Rev. E* **50**, 3878 (1994).
- [54] In the original paper, the relation of  $D_f$  with  $D_p$  presents a mistake that we corrected here.
- [55] H. Hentschel and I. Procaccia, *Physica D* **8**, 435 (1983).